Mathematical modelling of heating and evaporation of a spheroidal droplet

V.S. Zubkov [a,*], G.E. Cossali [b], S. Tonini [b], O. Rybdylova [a], C. Crua [a], M. Heikal [a], S.S. Sazhin [a]

[a] *Advanced Engineering Centre, School of Computing, Engineering and Mathematics, University of Brighton, Brighton BN2 4GJ, UK*
[b] *Department of Engineering and Applied Sciences, University of Bergamo, Viale Marconi 5, 24044 Dalmine, BG, Italy*

ABSTRACT

Most of the currently used models for droplet heating and evaporation are based on the assumption that droplets are perfect spheres. At the same time the shapes of many observed droplets in engineering applications are far from spherical. We have studied the influence of droplet non-sphericity on their heating and evaporation, approximating droplet shapes as prolate and oblate spheroids. The previously developed exact solutions to the heat and mass transfer equations for the gas phase surrounding a spheroidal droplet have been used as boundary conditions for the solutions to these equations in the liquid phase. The temperature gradients inside and at the surface of the droplets, and the changes in their shape during the heating and evaporation process have been taken into account. The effects of surface tension and droplet motion on droplet heating and evaporation are ignored. The results are applied to the analysis of heating and evaporation of an n-dodecane fuel droplet in Diesel engine-like conditions. The effect of droplet non-sphericity is shown to be relatively small for the evaporation time of these droplets with initial eccentricities $2/3 \leqslant \varepsilon \leqslant 1.5$.

1. Introduction

Most of the models for droplet heating and evaporation developed so far have been based on the assumption that droplets are perfect spheres [1]. At the same time the shapes of most actually observed droplets in engineering and environmental applications are far from spherical [2,3]. The effects of droplet deformation are generally investigated assuming that the droplet shapes can be approximated as prolate or oblate spheroids [4].

To the best of our knowledge, the heat conduction equation inside a spheroidal body (droplet) was first solved analytically more than 135 years ago [5]. This solution, however, turned out to be too complex for most practical applications. In most cases this problem (and the related problem of mass transfer inside the body) has been investigated based on the numerical solutions to heat transfer (and mass diffusion) equations [6,7].

The problem of heat/mass transfer inside spheroidal bodies, considered in the above-mentioned papers, is complementary to the problem of heat/mass transfer between the ambient gas and a spheroidal body, taking into account their relative velocity. The latter problem has been considered in numerous papers based on the numerical solutions to the momentum and heat transfer equations in the ambient gas in the ellipsoidal coordinate system. The analyses of [8–12] were based on the assumption that the body surface temperature was fixed. Juncu [13] took into account changes in body temperature with time, while assuming that there is no temperature gradient inside the body (the thermal conductivity of the body was assumed to be infinitely high).

These approaches are equally applicable to solid bodies and droplets. In the case of droplets, however, both heating and evaporation processes should be taken into account. Grow [14] was perhaps the first to solve the problem of heat and mass transfer in the vicinity of spheroidal particles assuming that their relative velocities are equal to zero, although she considered coal chars rather than droplets. One of the main limitations of that paper is that both mass and heat transfer equations were presented in the form of the Laplace equations, which implies that the effects of the Stefan flow from the surface of the particles were ignored. The latter effects were taken into account in the exact solutions to the mass and heat transfer equations in the gas phase around a spheroidal droplet in the model suggested in [4]. In that paper it was assumed that the temperatures at all points on the surface of the droplet are identical and constant, and that the droplet's shape remains the same. A combined problem of spheroidal droplet heating and evaporation, similar to the one studied in [4], was considered in [15]. As in [4], the authors of [15] based their analysis on the solution to the

* Corresponding author.
  E-mail address: V.Zubkov@brighton.ac.uk (V.S. Zubkov).

Nomenclature

A	area [m^2]
a	function defined by Eq. (3)
a_r	half the size of a spheroid perpendicular to the z-axis [m]
a_z	half the size of a spheroid along the z-axis [m]
B	function defined by Eq. (56)
c	specific heat capacity [J/kg K]
D_v	binary diffusion coefficient of vapour in air [m^2/s]
F	mass flux
G	non-dimensionalised evaporation rate
h	convective heat transfer coefficient [W/(m^2 K)]
H	specific enthalpy
J	diffusive mass flux
k	thermal conductivity [W/(m K)]
K	function defined by Eq. (59)
Le	Lewis number [–]
M	molar mass [kg/mol]
$\dot{m}_{ev}$	average mass evaporation rate [kg/s]
$\dot{m}$	local mass evaporation rate [kg/s]
$\mathbf{n}$	unit vector normal to the droplet surface [–]
P	gas pressure [bar]
P_{sat}	saturated vapour pressure [bar]
q	heat flux due to evaporation [W/m^2]
$\tilde{q}$	heat flux [W/m^2]
Q	heat rate [W]
R	effective droplet radius [m]
R_u	universal gas constant [J/(K mol)]
s	$s = 1$ for prolate spheroids, $s = -1$ for oblate spheroids
S	function defined by Eq. (5)
t	time [s]
t_{diff}	relative droplet evaporation time [%]
T	temperature [K]
T_0	initial uniform droplet temperature [K]

$\mathbf{U}$	Stefan velocity of the mixture of vapour and air [m/s]
v_n	normal velocity of the evaporating surface of the droplet [m/s]
W	correction factor defined by Eq. (47) [–]
x, y, z	Cartesian coordinates [–]
Y	mass fraction [–]
Z_1, Z_2	functions defined by Eq. (60)

Greek symbols

Γ	evaporation enhancement defined by Eq. (8)
ε	eccentricity (droplet deformation parameter) [–]
θ	angle [rad]
η	function defined by Eq. (11)
ξ, u, φ	ellipsoidal coordinates [–]
ρ	density [kg/m^3]
Φ	function defined by Eq. (2)
ζ	function defined by Eq. (11)

Subscripts

0	initial
a	air
c	critical
def	deformed (oblate or prolate)
eff	effective
f	liquid fuel
g	gas mixture (air and vapour)
p	at constant pressure
s	surface of droplet
sph	spherical
tot	mixture of gases, i.e. vapour and ambient air
v	vapour
∞	ambient gas (far from the droplet)

species conservation equation in the gas phase and assumed that the thermal conductivity of droplets is infinitely large. In contrast to [4], the authors of [15] took into account the relative velocities of droplets, assuming that the dependence of the Nusselt and Sherwood numbers on the Reynolds and Prandtl numbers is the same as for spherical droplets. Also, they took into account the time dependence of droplet temperatures and sizes, although their analysis was focused on oblate droplets only.

As follows from the above brief overview, a self-consistent model of heating and evaporation of spheroidal droplets is far from being developed. We believe, however, that the results presented in [4] could be considered as a starting point for constructing this model, at least for droplets that are almost spherical (slightly deformed spheres). In this paper we present the development of this new model.[1]

Our model is based on several simplifications, the most significant of which is the assumption that the droplet remains spheroidal during the heating and evaporation process, although the parameters of the spheroid, including its eccentricity, are allowed to change with time. The changes in the droplet parameters are attributed to the heating and evaporation processes only, not to the droplet oscillations driven by the surface tension. These assumptions do not allow us to apply the model to realistic moving and oscillating droplets, but we believe that our model can be considered an important step in this direction. It removes many assumptions made in previously proposed models [4]. Note that

the effect of oscillations on the heating and evaporation process can be ignored if the characteristic period of droplet oscillation is much longer than the droplet heating and evaporation time [4]. This is expected in extreme operating conditions that include low values of surface tension, large droplets, low latent heat of evaporation and/or high ambient temperatures.

The main ideas of the model described in [4] and its possible generalisations are summarised in the next section.

2. Gas phase

We start with a brief overview of the analysis reported in [4], which was focused on exact solutions to the mass and heat transfer equations in the gas phase around a spheroidal droplet, assuming a uniform Dirichlet boundary condition along the droplet surface. The model will be generalised to account for non-uniform conditions on the droplet surface, assuming that the gradients of temperature and vapour density perpendicular to the droplet surface are much greater than those along the droplet surface.

In [4] a droplet was assumed to be mono-component and the following steady-state equation for the vapour mass fraction ($Y_v = \rho_v/\rho_{\text{tot}}$) was solved in the gas phase:

$$\nabla(\rho_{\text{tot}}\mathbf{U}Y_v - \rho_{\text{tot}}D_v\nabla Y_v) = 0, \tag{1}$$

where $\rho_{\text{tot}} = \rho_v + \rho_a$ is the density of the mixture of vapour (with density ρ_v) and ambient air (with density ρ_a), $\mathbf{U}$ is the Stefan velocity of the mixture of vapour and air, D_v is the diffusion coefficient of vapour in air.

---

[1] The preliminary results were presented in our conference paper [16]; some minor mistakes made in the formulae and plots in the latter paper will be corrected.

Eq. (1) was solved using spheroidal coordinates ξ, u, φ defined as:

$$\begin{cases} x = a\Phi_-(\xi)\sin(u)\cos(\varphi), \\ y = a\Phi_-(\xi)\sin(u)\sin(\varphi), \\ z = a\Phi_+(\xi)\cos(u), \end{cases}$$

where

$$\Phi_\pm(\xi) = \frac{e^\xi \pm s(\varepsilon)e^{-\xi}}{2}, \quad s(\varepsilon) = \text{sign}(\varepsilon - 1), \quad \varepsilon = a_z/a_r, \tag{2}$$

$2a_z$ and $2a_r$ are the sizes of the spheroid along and perpendicular to the z-axis, respectively ($\varepsilon > 1$ and $s = 1$ for prolate spheroids, $0 < \varepsilon < 1$ and $s = -1$ for oblate spheroids).[2] It can be shown that the coordinate u is linked with $\theta = \arctan\left[\sqrt{x^2 + y^2}/z\right]$ by the relation $\tan u = \varepsilon \tan\theta$, which is valid for both prolate and oblate spheroids.

In this coordinate system the spheroidal surface is defined by the equations:

$$\xi = \xi_0 = \ln\sqrt{\frac{\varepsilon^s + 1}{\varepsilon^s - 1}}; \quad a = R_0 \frac{|1 - \varepsilon^2|^{1/2}}{\varepsilon^{1/3}}, \tag{3}$$

where R_0 is the radius of a sphere which has the same volume as the spheroid.

The authors of [4] solved Eq. (1) assuming that the values of Y_v and all other scalar properties are the same along the whole surface of the droplet and equal to $Y_v = Y_{vs}$, and Stefan velocity and diffusive fluxes are perpendicular to the droplet surface $\left(\mathbf{U} = (U_\xi, 0, 0), \nabla Y_v = \left(\frac{dY_v}{d\xi}, 0, 0\right)\right)$. These assumptions allowed the authors of [4] to simplify Eq. (1) to:

$$\rho_{tot} U_\xi \frac{dY_v}{d\xi} = \frac{D_v}{aS^2} \frac{d}{d\xi}\left[\rho_{tot}\Phi_-(\xi)\frac{dY_v}{d\xi}\right], \tag{4}$$

where

$$S^2 \equiv S^2(\xi, u) = \Phi_-(\xi)\left[\Phi_-^2(\xi)\cos^2 u + \Phi_+^2(\xi)\sin^2 u\right]^{1/2}. \tag{5}$$

Note that Eq. (4) is different from the one on which the analysis of [15] was based (see their Eq. (10)). The latter equation was the Laplace-type equation which is valid only in the case when the effect of the Stefan flow is ignored.

Eq. (4) was solved assuming that at large distances from the droplet $Y_v = Y_{v\infty} = $ const, and the condition $\rho_{tot} = \rho_v + \rho_a = $ const is valid (see [1]). The assumption $\rho_{tot} = \rho_v + \rho_a = $ const was relaxed in [17].

Average evaporation mass rate ($\dot{m}_{ev}$) and local evaporation mass rate per unit area (vapour mass flux) ($d\dot{m}/dA$) were found as [4]:

$$\dot{m}_{ev} = 4\pi R_0 \rho_{tot} D_v \Gamma(\varepsilon) \ln\frac{1 - Y_{v\infty}^{(v)}}{1 - Y_{vs}^{(v)}}, \tag{6}$$

$$\frac{d\dot{m}}{dA} = \frac{\varepsilon^{2/3}}{|1 - \varepsilon^2|S^2(\xi, u)R_0} \rho_{tot} D_v \Gamma(\varepsilon) \ln\frac{1 - Y_{v\infty}^{(v)}}{1 - Y_{vs}^{(v)}}, \tag{7}$$

where

$$\Gamma(\varepsilon) = \frac{|1 - \varepsilon^2|^{1/2}}{\varepsilon^{1/3}} \begin{cases} \frac{1}{\pi - 2\arctan\left(\sqrt{\frac{1+\varepsilon}{1-\varepsilon}}\right)} & \text{oblate} \\ \frac{1}{\ln\left(\sqrt{\frac{1+\varepsilon}{\varepsilon-1}}+1\right) - \ln\left(\sqrt{\frac{1+\varepsilon}{\varepsilon-1}}-1\right)} & \text{prolate}. \end{cases} \tag{8}$$

As mentioned earlier, in [4] it was assumed that $Y_{vs} = $ const. In the general case, these formulae could be applied when $Y_{vs} = Y_{vs}(u)$ provided that the gradients of Y_v in the direction perpendicular to the droplet surface are much larger than those along the surface. This condition is expected to be satisfied when the spheroid is a slightly deformed sphere (ε is close to 1).

The generalisation of the approach suggested in [17] to the case of spheroidal droplets has not been considered so far to the best of our knowledge.

Under the above-mentioned assumptions, the energy conservation equation was presented as (see Appendix A):

$$\rho_{tot}\mathbf{U}c_{pv}\nabla T = k_g\nabla^2 T, \tag{9}$$

where c_{pv} is the vapour specific heat capacity at constant pressure and k_g is the thermal conductivity of gas (a mixture of fuel vapour and air in the general case). Note that this equation is different from the one used in [4] (see Appendix A for the details).

This equation was solved using spheroidal coordinates for uniform temperature distributions along the droplet surface, assuming that the temperature at a large distance from the droplet is equal to $T_\infty = $ const. The solution for the temperature distribution in the gas phase was obtained in the form:

$$T = \frac{T_\infty - T_s}{1 - \eta}\left[\eta^{\zeta(\xi,\varepsilon)} - \eta\right] + T_s, \tag{10}$$

where

$$\eta = \exp\left[-\frac{1}{Le_v}\ln\frac{1 - Y_{v\infty}}{1 - Y_{vs}}\right], \tag{11}$$

$$\zeta(\xi, \varepsilon) = \begin{cases} \frac{\pi - 2\arctan(e^\xi)}{\pi - 2\arctan\left(\sqrt{\frac{1+\varepsilon}{1-\varepsilon}}\right)} & \text{oblate} \\ \frac{\ln(e^\xi + 1) - \ln(e^\xi - 1)}{\ln\left(\varepsilon + \sqrt{\varepsilon^2 - 1}\right)} & \text{prolate}, \end{cases}$$

$Le_v = k_g/(\rho_{tot}c_{pv}D_v)$ is the Lewis number for fuel vapour. Eq. (10) is identical to one derived by [4] when c in [4] is replaced with c_{pv}. The assumption that Y_v is the same along the whole surface of the droplet, used for the derivation of Eq. (4), implies that the tangential component of the temperature gradient along the surface of the droplet is nil. This is consistent with the assumption made by [4] that droplet thermal conductivity is infinitely large.

Considering heat transfer from an evaporating droplet, essentially the same analysis as presented above can be repeated, using the weaker assumption that the temperature gradients in the directions perpendicular to the droplet surface are much larger than along this surface (cf. the generalisation of the analysis by [4] for Y_v discussed earlier). In this case η becomes a function of u in the general case (recall that $Y_{vs} = Y_{vs}(T_s)$).

Expression (10) allows us to find the local convective heat transfer coefficient h based on the following formula:

$$h = -\frac{\left|-k_g\nabla T\right|_{\xi=\xi_0}}{|T_\infty - T_s|}. \tag{12}$$

Although the value of h was not explicitly calculated in [4], this calculation follows in a straightforward way from the previous analysis by these authors:

$$h = \frac{-k_g\eta\ln\eta}{R_0(1-\eta)} \begin{cases} \frac{\varepsilon^{1/3}}{\left[\pi - 2\arctan\left(\sqrt{\frac{1+\varepsilon}{1-\varepsilon}}\right)\right]\sqrt{\left(\frac{1}{1-\varepsilon^2} - \sin^2 u\right)}} & \text{oblate} \\ \frac{\varepsilon^{1/3}}{\left[\ln\left(\varepsilon + \sqrt{\varepsilon^2 - 1}\right)\right]\sqrt{\left(\frac{1}{\varepsilon^2 - 1} + \sin^2 u\right)}} & \text{prolate} \end{cases} \tag{13}$$

where η is defined by Expression (11). This equation can be rearranged as:

---

[2] Note that in [11,12] prolate and oblate spheroids were defined as those with $\varepsilon < 1$ and $\varepsilon > 1$, respectively; the same definition is used in Fig. 1 of [10].

$$h = \frac{-k_g \eta \ln \eta}{R_0(1-\eta)} \varepsilon^{1/3} \left[\left\{ \begin{array}{ll} \frac{\sqrt{1-\varepsilon^2}}{\left[\pi - 2\arctan\left(\sqrt{\frac{1+\varepsilon}{1-\varepsilon}}\right)\right]} & \text{oblate} \\ \frac{\sqrt{\varepsilon^2-1}}{\left[\ln\left(\varepsilon+\sqrt{\varepsilon^2-1}\right)\right]} & \text{prolate} \end{array} \right. \right] \sqrt{\frac{1+\varepsilon^2\tan^2\theta}{1+\varepsilon^4\tan^2\theta}}.$$

(14)

Perhaps the most important limitation of the model summarised above is that it does not take into account the changes in the shape of the droplets during the evaporation process. A simplified model, taking into account these changes and predicting the time evolution of redistribution of the temperature inside droplets is described in the next section.

3. Liquid phase

For the liquid phase, the transient heating of an evaporating droplet is described by the following equation:

$$\rho_f c_f \frac{\partial T}{\partial t} - \nabla(k_f \nabla T) = 0,$$

(15)

where k_f, ρ_f, and c_f are thermal conductivity, density and specific heat capacity, respectively, of liquid fuel. The analytical solution for the gas phase around a spheroidal droplet, presented in [4] and discussed above, is used for the boundary condition at the droplet surface:

$$-\mathbf{n}(-k_f \nabla T) = q + h(T_\infty - T) \quad \text{at} \quad \xi = \xi_0,$$

(16)

where $\mathbf{n}$ is the unit vector normal to the droplet surface, the convective heat transfer coefficient h is defined by (14) and q is the heat flux due to evaporation to be specified later.

We take into account the decrease in the droplet size due to evaporation but not the effect of thermal swelling. The shape of the droplet is recalculated at each time step assuming that the droplet remains spheroidal. The dimensions of the droplet along and perpendicular to the z-axis are described by the following ordinary differential equations

$$a_r'(t) = -\frac{1}{\rho_f}\frac{d\dot{m}}{dA}\bigg|_{u=\pi/2}, \quad a_z'(t) = -\frac{1}{\rho_f}\frac{d\dot{m}}{dA}\bigg|_{u=0},$$

(17)

and initial conditions

$$a_r(0) = a_{r0}, \quad a_z(0) = a_{z0},$$

where evaporation mass flux $\frac{d\dot{m}}{dA}$ varies along the droplet surface; it is defined by Eq. (7). Temperature, T, and the vapour density, ρ_v, at the droplet surface are linked by the ideal gas law

$$\rho_{vs} = \frac{M_v P_{sat}}{R_u T_s}.$$

(18)

We assume that $\rho_{v\infty} = 0$. The ideal gas law is also used for air density near the droplet surface and in ambient conditions:

$$\rho_{as} = \frac{M_a(P - P_{sat})}{R_u T_s}, \quad \rho_{a\infty} = \frac{M_a P}{R_u T_\infty},$$

(19)

where P is the ambient gas pressure and P_{sat} is the saturated vapour pressure, R_u is the universal gas constant, M_v and M_a are molar masses of the vapour and the ambient air, respectively.

Our model is based on the assumption that at each stage of heating and evaporation, the droplet shape can be approximated by that of a spheroid but with time dependent a_r and a_z. The initial distribution of the temperature is assumed to be uniform inside the droplet, $T = T_0$, and the temperature in the ambient gas, T_∞, is assumed to be constant.

The effects of surface tension and droplet oscillations on heating and evaporation processes are ignored. It is assumed that the droplet does not move relative to air.

4. Parameters of the model and numerical method

Our analysis will be focused on Diesel fuel droplet heating and evaporation in Diesel engine-like conditions, in view of our specific interest in modelling the processes in these engines (the results of our previous analysis are quite general and are expected to be used in a much wider range of applications). Diesel fuel is approximated by n-dodecane $C_{12}H_{26}$, although the limitations of this approximation are well known [18]). Following [19,20], we define the saturated vapour pressure, the diffusion coefficient of vapour in air, thermal conductivity of liquid fuel, the specific heat capacity of liquid fuel and fuel vapour, and the heat flux due to evaporation for n-dodecane as

$$P_{sat*} = \exp\left(8.1948 - 7.8099(300/T_s) - 9.0098(300/T_s)^2\right) \quad \text{(bar)},$$

(20)

$$P_{sat} = \begin{cases} P_{sat*} & \text{when } T_s \leqslant 0.99 T_{cr} \\ \exp\left(15(T_s - 0.99 T_{cr})/0.99 T_{cr}\right) P_{sat*} & \text{when } T_s > 0.99 T_{cr} \end{cases},$$

(21)

$$D_v = 5.27 \cdot 10^{-6} (T_{\text{eff}}/300)^{1.583} P^{-1} \quad (\text{m}^2/\text{s}) \text{ (P in bar)},$$

(22)

$$T_{\text{eff}} = \frac{2T_s + T_\infty}{3},$$

(23)

$$k_f = 0.1405 - 0.00022(T - 300) \quad \text{(W/m K)},$$

(24)

$$c_f = 2.18 + 0.0041(T - 300) \quad \text{(kJ/kg K)},$$

(25)

$$c_{pv} = 0.2979 + 1.4394(T_{\text{eff}}/300) + 0.1351(T_{\text{eff}}/300)^2 \quad \text{(kJ/kg K)},$$

(26)

$$q = 37.44 \cdot 10^3 (T_{cr} - T)^{0.38} \rho_f v_n,$$

(27)

where T_{eff} and T_{cr} (in K) are the effective (using the 1/3 rule) and critical temperatures, v_n is the normal velocity of the recession of the evaporating surface of the droplet (see Appendix B),

$$v_n = v_r n_r + v_z n_z,$$

(28)

$$v_r = -r(r^2 a_r'/a_r^3 + z^2 a_z'/a_z^3), \quad v_z = z(r^2 a_r'/a_r^3 + z^2 a_z'/a_z^3),$$

(29)

$$\begin{cases} n_r = -r/a_r^2 \sqrt{r^2/a_r^4 + z^2/a_z^4}, \\ n_z = -z/a_z^2 \sqrt{r^2/a_r^4 + z^2/a_z^4}. \end{cases}$$

(30)

Assuming that the contribution of fuel vapour to the thermal conductivity of the mixture of vapour and air can be ignored, we can approximate empirical data given in [21] by the following function:

$$k_g = 0.0036 + 0.0252(T_{\text{eff}}/300) - 0.00189(T_{\text{eff}}/300)^2 \quad \text{(W/m K)}.$$

(31)

The values of other parameters used in our analysis are presented in Table 1.

Eqs. (15)–(17) were solved numerically until the droplet effective radius, R, dropped below $5 \cdot 10^{-8}$ m. They were integrated using the finite-element-based PDE modules of COMSOL Multiphysics including Moving Mesh (ALE). We ensured that the solutions remained unaffected by the mesh size and time steps below certain minimal values.

Table 1
The values of the parameters used in the analysis.

Parameter	Value	Notes
ε_0	1.5 (2/3)	Initial droplet deformation for prolate (oblate) droplet
R_0	10^{-5} m	Initial effective droplet radius
ρ_f	744.11 kg/m^3	Liquid n-dodecane (C$_{12}$H$_{26}$) density
T_0	300 K	Initial droplet temperature
T_∞	700 K	Ambient gas temperature
P	30 bar	Ambient gas pressure
R_u	8.3154 J/(K mol)	Universal gas constant
M_v	$170.33 \cdot 10^{-3}$ kg/mol	Molar mass of vapour
M_a	$28.97 \cdot 10^{-3}$ kg/mol	Molar mass of ambient air
T_{cr}	659 K	Critical n-dodecane temperature

5. Results

In this section, we consider the results of numerical solutions to Eqs. (15)–(17), describing heating and evaporation of a stagnant spheroidal droplet surrounded by air. Functionality testing of the model was carried out to ensure that the solution for spherical droplets, using the previously developed approach [22], agrees with the predictions of the newly developed model in the limiting case when spheroidal droplets become spherical ($\varepsilon \to 1$) (see Appendix C).

In Fig. 1, the temperature profiles along the vertical cross section of a prolate evaporating droplet at four time instants are shown. The initial droplet deformation parameter is assumed equal to $\varepsilon_0 = 1.5$ and the initial effective radius $R_0 = 10^{-5}$ m. As follows from Fig. 1B, the temperatures inside the droplet and at its surface increase over time and reach their highest values at the spheroid's extremities (poles) where the surface curvature is the greatest. As a result of higher evaporation in these regions of the droplet surface, the shape of the droplet becomes more spherical with time. Similar

qualitative behaviour is shown in Fig. 2 for an evaporating oblate droplet with initial deformation parameter $\varepsilon_0 = 2/3$ and an initial effective radius $R_0 = 10^{-5}$ m.

Fig. 3A shows a schematic of a prolate droplet with an initial deformation parameter $\varepsilon_0 = 1.5$; a_r and a_z are the radial and axial semi-axes. Fig. 3B-D demonstrates how characteristics of the prolate (solid lines) and oblate (dashed lines) spheroids change with time. Fig. 3D shows that the evaporation at the droplet surface regions with higher curvature (e.g. point B in Fig. 3A for a prolate droplet) is higher than at point A (by up to 700%). Higher evaporation means that droplet eccentricity will move towards 1 (see Fig. 3B). This suggests that the evaporation of a droplet causes it to become more spherical. In Fig. 3C, we demonstrate that local temperatures at point A (T_A) and point B (T_B), of the deformed droplet surface can vary noticeably (by up to more than 35 K). Using (17) for constant temperature along the droplet surface, we obtain, $a_z'/a_r' = \varepsilon$. Thus, once the temperature along the droplet surface becomes uniform (or close to uniform), the ratio $a_z'/a_r' = \varepsilon$. Furthermore, it can be shown analytically that the droplet shape remains ellipsoidal when the droplet temperature is uniform (see Appendix D). Note that in our analysis this temperature is not uniform in the general case (see Fig. 3B).

Fig. 4 shows how the effective radius of prolate (solid), oblate (dashed) and spherical (dotted) droplets changes with time due to evaporation (curves for prolate and oblate droplets are indistinguishable). This figure demonstrates that prolate and oblate droplets, with initial effective radius $R_0 = 10^{-5}$ m and initial deformation parameters $\varepsilon_0 = 1.5$ and $\varepsilon_0 = 2/3$, evaporate slightly faster (by 1.4%) than a spherical droplet with the same initial volume (same R_0).

Note that the results shown in Figs. 1(D) and 2(D) should be viewed with caution as for very small droplets kinetic, molecular dynamics and even quantum chemical effects, ignored in our analysis, are likely to become important [20,23,24].
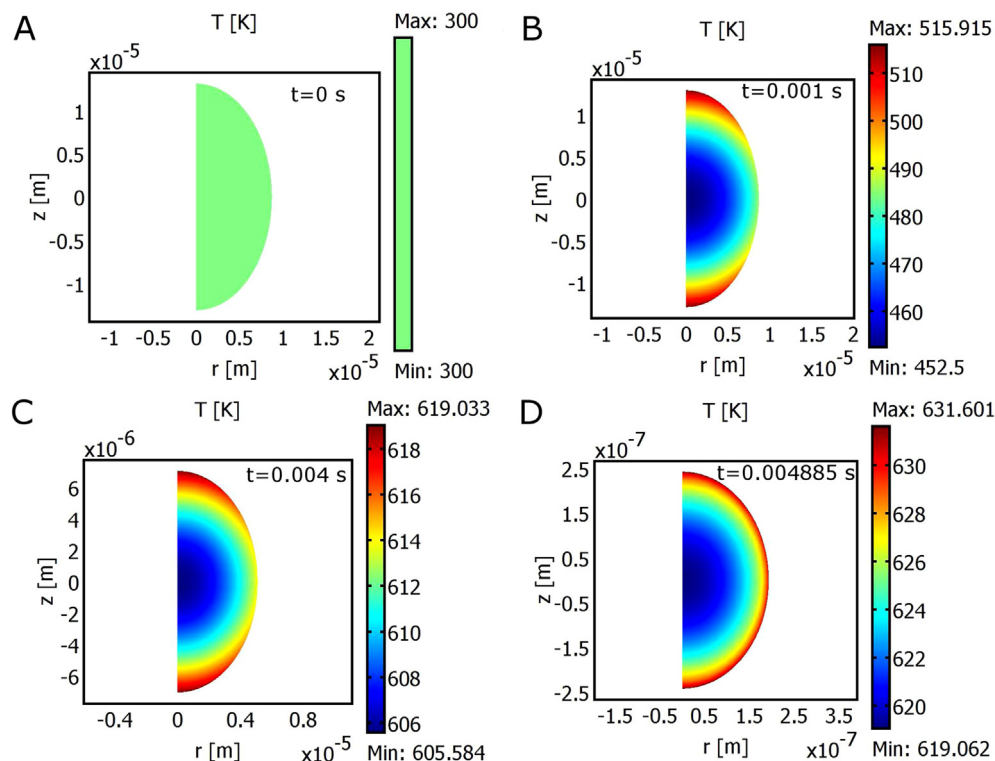

Fig. 1. Temperature profiles along the vertical cross section of a prolate droplet at four instants of time: (A) $t = 0$ s, (B) $t = 0.001$ s, (C) $t = 0.004$ s, (D) $t = 0.004885$ s. Droplet initial temperature, $T_0 = 300$ K; ambient gas temperature, $T_\infty = 700$ K; gas pressure, $P = 30$ bar.
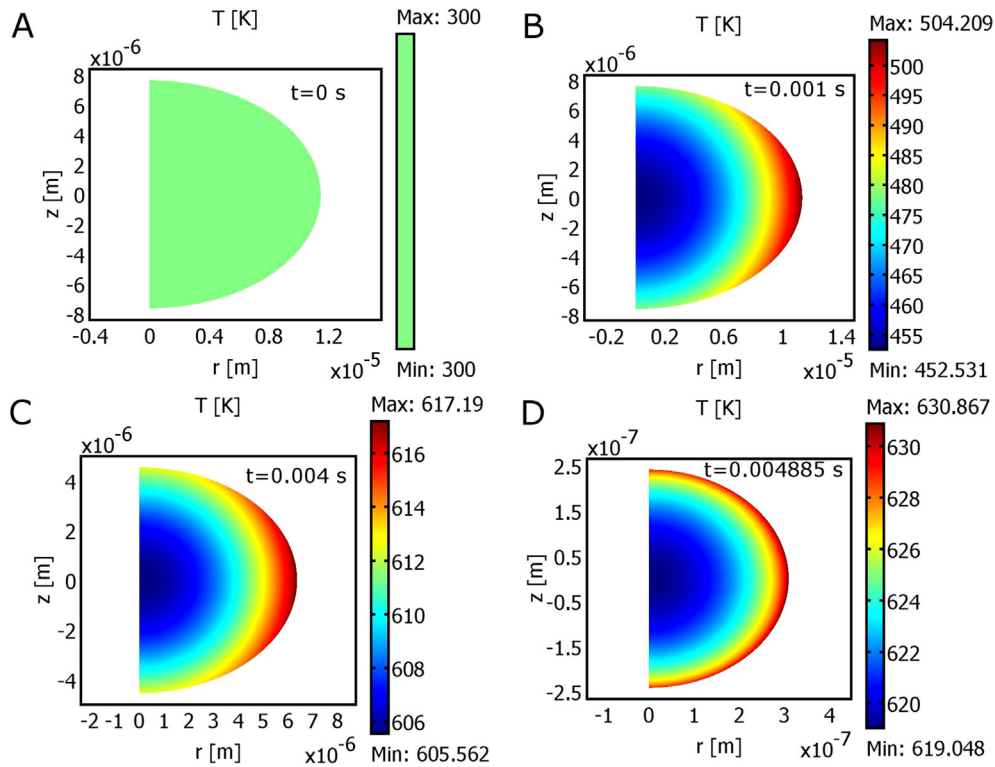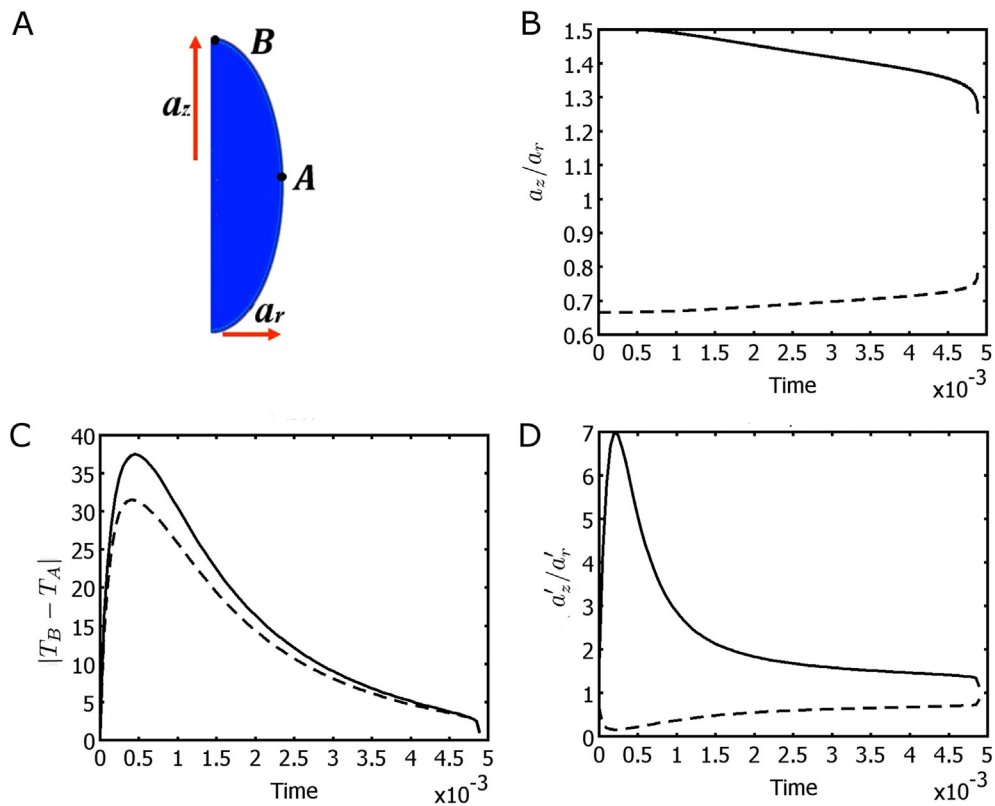
Fig. 2. Temperature profiles along the vertical cross section of an oblate droplet at four instants of time: (A) $t = 0$ s, (B) $t = 0.0001$ s, (C) $t = 0.004$ s, (D) $t = 0.004885$ s. Drop initial temperature, $T_0 = 300$ K; ambient gas temperature, $T_\infty = 700$ K; gas pressure, $P = 30$ bar.

Fig. 3. (A) A schematic of a prolate droplet with an initial deformation parameter $\varepsilon_0 = 1.5$; a_r and a_z are the radial and axial droplet semi-axes; (B) ratio $\varepsilon = a_z/a_r$ versus time (s) for prolate (solid) and oblate (dashed) droplets; (C) absolute value of the temperature difference (in K) at points A and B of prolate (solid) and oblate (dashed) droplets versus time (s); T_A and T_B are surface temperatures at points A and B, respectively; (D) ratio a'_z/a'_r vs time for prolate (solid) and oblate (dashed) droplets. Droplet initial temperature, $T_0 = 300$ K; ambient gas temperature, $T_\infty = 700$ K; gas pressure, $P = 30$ bar.
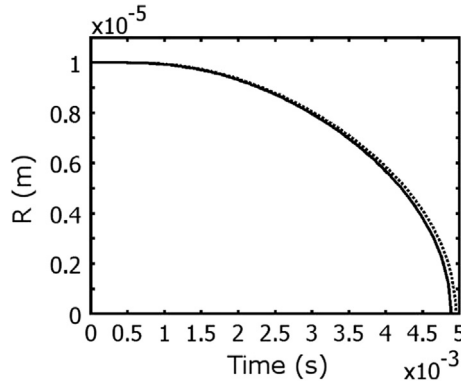
Fig. 4. Effective radii of prolate (solid), oblate (dashed) and spherical (dotted) droplets versus time during the heating and evaporation processes. Droplet initial temperature, $T_0 = 300$ K; surrounding gas temperature, $T_\infty = 700$ K; gas pressure, $P = 30$ bar.

5.1. Parameter sensitivity analysis

We analysed the sensitivity of the model to deviations in the key parameters shown in Table 1. We introduce t_{diff} characterising the relative evaporation time difference between spherical and deformed droplets,

$$t_{diff} = (t_{sph} - t_{def})/t_{sph} \cdot 100\%, \tag{32}$$

where t_{sph} and t_{def} are evaporation times of the spherical and deformed droplets, respectively. Fig. 5 shows how t_{diff} is influenced by changes in parameters R_0 (its default value is $1 \cdot 10^{-5}$ m; the range of values $[2 \cdot 10^{-6}$ m, $2 \cdot 10^{-5}$ m] was considered), T_∞ (its default value is 700 K, the range of values [500 K, 900 K] was considered), T_0 (its default value is 300 K, the range of values [300 K, 500 K] was considered) and P (its default value is 30 bar, the range of values [5 bar, 60 bar] was considered).

The results of our analysis demonstrate that t_{diff} changes only in the range 1–3%; there is no visible dependence of t_{diff} on R_0 for

prolate droplets. Thus, the evaporation time difference t_{diff} shows almost no sensitivity to variations in these parameters and t_{diff} for spherical and deformed droplets was shown to be small.

6. Conclusions

A new mathematical model for heating and evaporation processes of a liquid spheroidal (prolate and oblate) droplet is described.

The previously obtained exact solutions to the heat and mass transfer equations for the gas phase surrounding a spheroidal droplet were used as boundary conditions for the solutions to these equations in the liquid phase. The temperature gradients, inside and at the surface of the droplets, and the changes in their shape during the heating and evaporation process were taken into account, assuming that the gradients of temperature perpendicular to the droplet surface are much larger than those along this surface. The results were applied to the analysis of heating and evaporation of an n-dodecane (approximation of Diesel fuel) droplet in Diesel engine-like conditions.

It is shown that local temperatures can vary noticeably along the droplet surface (by up to more than 35 K) and significant changes in local evaporation rates (by up to 700%) were observed. Droplet heating is shown to be more intense in the regions with greatest curvature.

Higher evaporation at the droplet surface in these regions led to a decrease in droplet eccentricity ($\varepsilon = a_z/a_r$) for prolate and an increase for oblate droplets. In both cases this eccentricity is shown to tend towards 1 at the end of the evaporation process (i.e. the droplet becomes more spherical).

The effect of droplet non-sphericity on the evaporation time of droplets was shown to be relatively small for the range of parameter values under consideration.
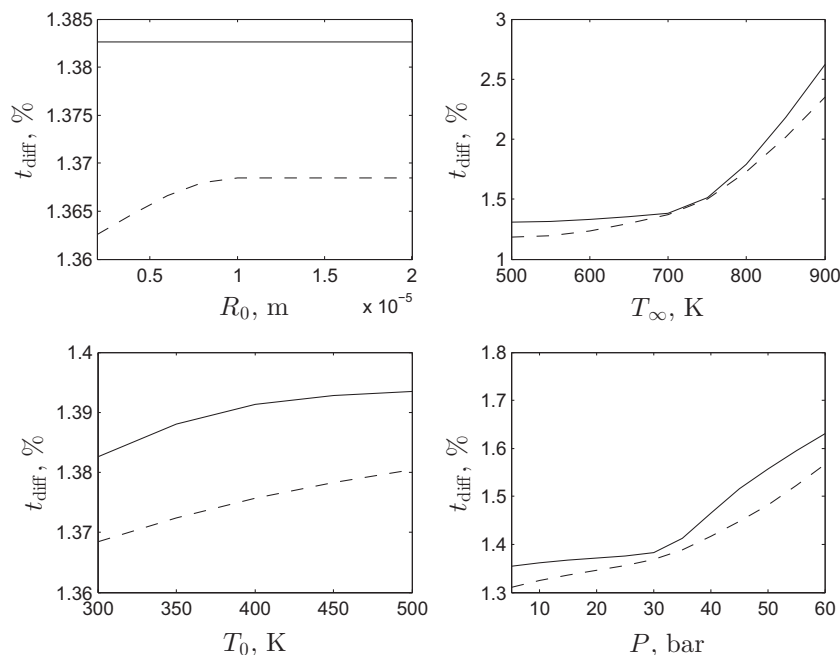
Acknowledgements

Fig. 5. The results of sensitivity analysis for four parameters: R_0, T_∞, T_0 and P. The relative differences in the droplet evaporation times for spherical and deformed droplets (prolate (solid) and oblate (dashed) spheroids), t_{diff}, are shown to be small (less than 3%).

Appendix A. Energy equation with inter-diffusional terms

We consider an energy transport process in a mixture of N gases. The steady-state energy equation for this mixture, taking into account inter-diffusional terms (but ignoring work and dissipation terms), can be presented as [25]:

$$\nabla_j(\rho_{tot}U_jH_{tot}) = -\nabla_j\tilde{q}_j - \nabla_j\sum_{i=0}^{N}H_iJ_j^{(i)}, \tag{33}$$

where H_i is the specific enthalpy of species i, $J_j^{(i)}$ is the jth component of the diffusive mass flux of species i; H_{tot}, k_{tot} and ρ_{tot} are the enthalpy, thermal conductivity and density of the gaseous mixture, respectively $\left(H_{tot} = \sum_{i=0}^{N}H_iY^{(i)}\right)$; U_j and $\tilde{q}_j = -k_{tot}\nabla_jT$ are the jth components of the velocity vector of the gaseous mixture and the heat flux, respectively.

Let us rewrite Eq. (33) in the form:

$$\nabla_j\left[\rho_{tot}U_j\sum_{i=0}^{N}H_iY^{(i)} + \sum_{i=0}^{N}H_iJ_j^{(i)}\right] = \nabla_j(k_{tot}\nabla_jT). \tag{34}$$

The left-hand side (LHS) of Eq. (34) can be rewritten as

$$\nabla_j\left[\rho_{tot}U_j\sum_{i=0}^{N}H_iY^{(i)} + \sum_{i=0}^{N}H_iJ_j^{(i)}\right] = \nabla_j\sum_{i=0}^{N}H_i\left(\rho_{tot}U_jY^{(i)} + J_j^{(i)}\right). \tag{35}$$

Introducing the total mass flux (sum of diffusive and convective fluxes)

$$F_j^{(i)} = \rho_{tot}U_jY^{(i)} + J_j^{(i)}, \tag{36}$$

the right-hand side of Eq. (35) can be presented as:

$$\nabla_j\sum_{i=0}^{N}H_i\left(\rho_{tot}U_jY^{(i)} + J_j^{(i)}\right) = \nabla_j\sum_{i=0}^{N}F_j^{(i)}H_i. \tag{37}$$

This allows us to present Eq. (33) as

$$\nabla_j\sum_{i=0}^{N}F_j^{(i)}H_i = \nabla_j(k_{tot}\nabla_jT). \tag{38}$$

This is the equation 'H' in Table 19.2-4 of [25] ($\sum_{i=0}^{N}F_j^{(i)}H_i$ in our paper is the same as $\sum_{i=0}^{N}N_j^{(i)}\bar{h}_i$ in [25], $\bar{h}_i$ is the partial molar enthalpy of species i).

In the case of a binary mixture of a vapour and a gas ($\mathbf{F}^{(v)} = \mathbf{F}^{(1)}$ and $\mathbf{F}^{(g)} = \mathbf{F}^{(0)}$), Eq. (38) is simplified to

$$\nabla_j\left(F_j^{(v)}H_v + F_j^{(g)}H_g\right) = \nabla_j(k_{tot}\nabla_jT). \tag{39}$$

Taking into account that the net ambient gas flux is zero (convective flux compensates for the diffusion flux), $\left(\mathbf{F}^{(g)} = 0\right)$, we have:

$$F_j^{(v)} = \rho_{tot}U_jY^{(v)} + J_j^{(v)}. \tag{40}$$

Remembering that [1]:

$$J_j^{(v)} = \rho_{tot}U_jY^{(g)}, \tag{41}$$

we can rewrite Eq. (39) as:

$$\nabla_j\rho_{tot}U_jH_v = \nabla_j(k_{tot}\nabla_jT). \tag{42}$$

Remembering that

$$H_v = c_{pv}T + H_{v0} \tag{43}$$

and the mass conservation equation ($\nabla\mathbf{U} = 0$) we obtain,

$$\rho_{tot}U_jc_{pv}\nabla_jT = \nabla_j(k_{tot}\nabla_jT). \tag{44}$$

Eq. (44) is identical to Eq. (10). This equation is the same as given in [4] if c in the latter paper is replaced with c_{pv}.

The solution to Eq. (44) yields (as in [26], except for the value of c_{pv}) the non-dimensionalised heat rate,

$$\tilde{Q}_s = \frac{Q_s}{4\pi R_0 kT_\infty} = \left(\frac{\tilde{T}_s - 1}{e^{\tilde{G}\Gamma(\varepsilon)} - 1}\right)\tilde{G}, \tag{45}$$

where $\tilde{T}_s = \frac{T_s}{T_\infty}$ is the non-dimensionalised surface temperature, $\tilde{G} = \frac{\dot{m}_{ev}c_{pv}}{4\pi R_0 k_{tot}}$ is the non-dimensionalised evaporation rate, $Q_s = -4\pi R_0^2 k_{tot}\nabla_nT$, and ∇_nT is the normal component of the temperature gradient. The analysis of the case without inter-diffusional terms (considered in [4]) would yield the same equation as (45) but with $\tilde{G}' = \frac{\dot{m}_{ev}c_{pg}}{4\pi R_0 k_{tot}} = \tilde{G}\frac{c_{pv}}{c_{pg}}$:

$$\tilde{Q}_s' = \left(\frac{\tilde{T}_s - 1}{e^{\tilde{G}'\Gamma(\varepsilon)} - 1}\right)\tilde{G}' = \left(\frac{\tilde{T}_s - 1}{e^{\tilde{G}\frac{c_{pv}}{c_{pg}}\Gamma(\varepsilon)} - 1}\right)\tilde{G}\frac{c_{pv}}{c_{pg}}$$
$$= \left(\frac{\tilde{T}_s - 1}{e^{\tilde{G}\Gamma(\varepsilon)} - 1}\right)\tilde{G}\left[\frac{c_{pv}}{c_{pg}}\frac{e^{\tilde{G}\Gamma(\varepsilon)} - 1}{e^{\tilde{G}\frac{c_{pv}}{c_{pg}}\Gamma(\varepsilon)} - 1}\right] = \tilde{Q}_sW, \tag{46}$$

where

$$W = \frac{c_{pv}}{c_{pg}}\frac{e^{\tilde{G}\Gamma(\varepsilon)} - 1}{e^{\tilde{G}\frac{c_{pv}}{c_{pg}}\Gamma(\varepsilon)} - 1} \tag{47}$$

is a correction factor. If $\tilde{G}$ is small,

$$e^{\tilde{G}\Gamma(\varepsilon)} = 1 + \tilde{G}\Gamma(\varepsilon) + O(\tilde{G}^2) \tag{48}$$

and $W = 1 + O(\tilde{G}^2)$. Thus, the solution to Eq. (10), considered in this paper, becomes close to the solution considered in [4].

Appendix B. Derivation of Eq. (29)

The normal velocity of the recession of the droplet evaporating surface used in Eqs. (27)–(29) can be presented as:

$$v_n = v_rn_r + v_zn_z, \tag{49}$$

$$v_r = -r(r^2a_r'/a_r^3 + z^2a_z'/a_z^3), \quad v_z = z(r^2a_r'/a_r^3 + z^2a_z'/a_z^3), \tag{50}$$

Note that the normal velocity of the recession of the droplet evaporating surface is related to the local mass evaporating flux, $\frac{d\dot{m}}{dA}$, as:

$$v_n(u) = -\frac{1}{\rho_f}\frac{d\dot{m}}{dA} \tag{51}$$

(cf. Eq. (17)).

We assumed that the evaporating droplet shape remains spheroidal. At each time step, we define the sizes (a_z and a_r) and their time derivatives (a_z' and a_r') along and perpendicular to the z-axis, using (17), and then calculate the evaporation flux at other points on the spheroidal droplet, using interpolation.

To derive Eq. (27), let us follow a point at the droplet surface (r_1, z_1) that moves to a point (r_2, z_2) at the deformed droplet surface due to evaporation when time changes from t_1 to t_2, assuming that t_1 is close to t_2. Taking into account the fact that points (r_1, z_1) and (r_2, z_2) are at the surfaces of spheroids with semi-axes a_{r1}, a_{z1} and a_{r2}, a_{z2}, respectively, we obtain,

$$\begin{cases} \left(\frac{r_1}{a_{r1}}\right)^2 + \left(\frac{z_1}{a_{z1}}\right)^2 = 1, \\ \left(\frac{r_2}{a_{r2}}\right)^2 + \left(\frac{z_2}{a_{z2}}\right)^2 = 1, \\ \frac{a_{r2}}{a_{r1}} = \frac{a_{z2}}{a_{z1}}. \end{cases} \tag{52}$$

Assuming that

$$\Delta a_r = a_{r2} - a_{r1}, \quad \Delta a_z = a_{z2} - a_{z1} \tag{53}$$

are small, and omitting second order terms in (52), we obtain

$$
\begin{cases}
r_2 - r_1 = -r_1 \left(\left(\frac{r_1}{a_{r1}} \right)^2 \Delta a_r + \left(\frac{z_1}{a_{z1}} \right)^2 \Delta a_z \right), \\
z_2 - z_1 = -z_1 \left(\left(\frac{r_1}{a_{r1}} \right)^2 \Delta a_r + \left(\frac{z_1}{a_{z1}} \right)^2 \Delta a_z \right).
\end{cases}
\tag{54}
$$

Dividing both parts of Eq. (54) by $t_2 - t_1$ and remembering that $t_2 - t_1 \to 0$, we obtain:

$$
\begin{aligned}
v_r|_{(r_1,z_1)} &= -r_1 (r_1^2 a'_{r1}/a_{r1}^3 + z_1^2 a'_{z1}/a_{z1}^3), \\
v_z|_{(r_1,z_1)} &= z (r_1^2 a'_{r1}/a_{r1}^3 + z_1^2 a'_{z1}/a_{z1}^3).
\end{aligned}
\tag{55}
$$

These expressions are identical to those given in Eq. (29).

Appendix C. Predictions of the new model and the one described in [22] for a spherical droplet

In what follows, the predictions of the model described in [22] for a spherical droplet are compared with the predictions of our model in the limit when the droplet deformation parameter (eccentricity) is equal to 1 (spherical droplet) and the other parameter values are as given in Table 1. Fig. 6 shows the effective radius of a droplet and its surface temperature, predicted by the model described in [22] (dashed) and our model (solid) versus time. In our model the droplet was assumed to be spherical when the deformation parameter ε was equal to 1.001. Fig. 6 demonstrates a reasonably good agreement between the predictions of both models, the difference between the results turned out to be less than about 3%. These differences are comparable with the accuracy of the models used in our analysis (the model used in [22] was based on the analytical solution to the heat transfer equation inside droplets at each time step, while our model was based on the numerical solution of this equation; the approximations of the transport and thermodynamics properties of the fluids used in both models were slightly different).

Appendix D. A simplified analysis of droplet shape evolution

Consider a point on a spheroidal surface (r_1, z_1), where $r_1 = \sqrt{x_1^2 + y_1^2}$, and evaluate the time derivative of the following parameter,

$$
B = \frac{r_1^2}{a_r^2} + \frac{z_1^2}{a_z^2}.
\tag{56}
$$

Note that initially $B = 1$. Differentiating (56) with respect to time gives

$$
\frac{1}{2} \frac{dB}{dt} = \frac{r_1 \dot{r}_1 a_r^2 - r_1^2 a_r \dot{a}_r}{a_r^4} + \frac{z_1 \dot{z}_1 a_z^2 - z_1^2 a_z \dot{a}_z}{a_z^4}.
\tag{57}
$$

Note that for a spheroid we have the following relations:

$$
\begin{aligned}
r_1 &= R_0 \varepsilon^{-1/3} \sin\theta_1; \quad z_1 = R_0 \varepsilon^{2/3} \cos\theta_1, \\
a_r &= R_0 \varepsilon^{-1/3}; \quad a_z = R_0 \varepsilon^{2/3}.
\end{aligned}
$$

The time derivative of (r_1, z_1) can be calculated as:

$$
(\dot{r}_1, \dot{z}_1) = -\frac{\dot{m}_{ev}}{4\pi R_0^2 \rho_f} K(\theta_1)(n_r, n_z),
\tag{58}
$$

where (n_r, n_z) are the radial and z-component of the unit vector normal to the surface:

$$
(n_r, n_z) = \frac{\left(\varepsilon^{2/3} \sin\theta, \varepsilon^{-1/3} \cos\theta \right)}{\left(\varepsilon^{-2/3} \cos^2\theta + \varepsilon^{4/3} \sin^2\theta \right)^{1/2}},
$$

$$
K(\theta_1) = \frac{\varepsilon^{2/3}}{\sqrt{1 + (\varepsilon^2 - 1)\sin^2(\theta_1)}},
\tag{59}
$$

$\frac{\dot{m}_{ev}}{4\pi R_0^2}$ is the average evaporation flux at the surface of the droplet. Eq. (58) can be rewritten in a more explicit form as:

$$
(\dot{r}_1, \dot{z}_1) = -\frac{\dot{m}_{ev}}{4\pi R_0^2 \rho_f} \frac{\left(\varepsilon^{5/3} \sin\theta_1, \varepsilon^{2/3} \cos\theta_1 \right)}{\left(1 + (\varepsilon^2 - 1)\sin^2\theta_1 \right)^{3/2}}.
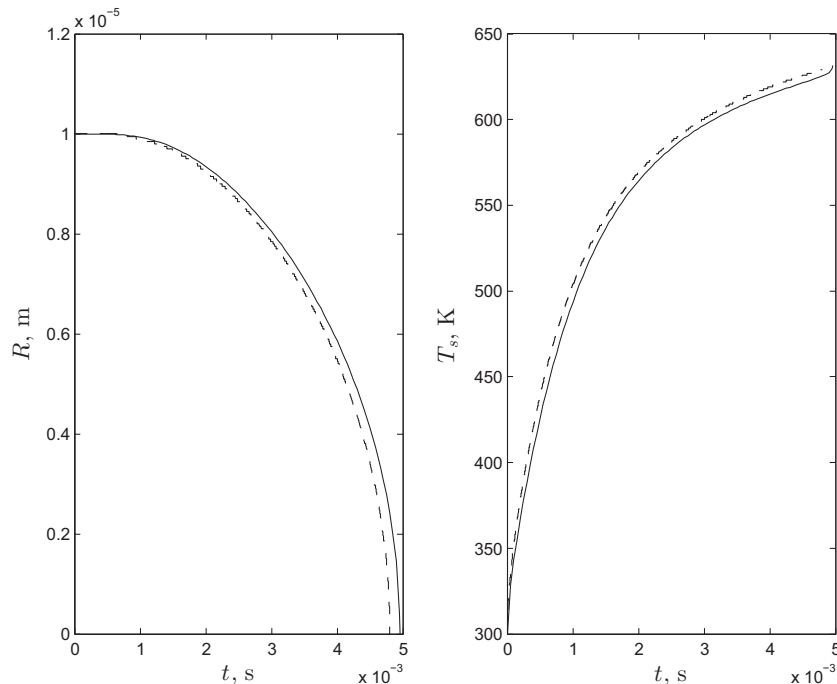$$

Fig. 6. Radii of a spherical droplet and its surface temperature as functions of time predicted by the model developed in this paper (solid) and the model described in [22] (dashed).

The time derivatives of the half-axes are estimated as:

$$\dot{a}_r = -\frac{v\left(\theta = \frac{\pi}{2}\right)}{\rho_f} = -\frac{\dot{m}_{ev}}{4\pi R_0^2 \rho_f} K\left(\frac{\pi}{2}\right) = -\frac{\dot{m}_{ev}}{4\pi R_0^2 \rho_f} \varepsilon^{-1/3}$$

$$\dot{a}_z = -\frac{v(\theta = 0)}{\rho_f} = -\frac{\dot{m}_{ev}}{4\pi R_0^2 \rho_f} K(0) = -\frac{\dot{m}_{ev}}{4\pi R_0^2 \rho_f} \varepsilon^{2/3}.$$

Thus the values of a_r, a_z, r_1 and z_1 and their derivatives can be presented as:

$$a_r = R_0 \varepsilon^{-1/3}; \quad a_z = R_0 \varepsilon^{2/3}$$

$$\dot{a}_r = -Z_1 \varepsilon^{-1/3}; \quad \dot{a}_z = -Z_1 \varepsilon^{2/3}$$

$$r_1 = R_0 \varepsilon^{-1/3} \sin\theta_1; \quad z_1 = R_0 \varepsilon^{2/3} \cos\theta_1$$

$$\dot{r}_1 = -Z_2 \varepsilon^{5/3} \sin\theta_1; \quad \dot{z}_1 = -Z_2 \varepsilon^{2/3} \cos\theta_1,$$

where

$$\begin{cases} Z_1 = \frac{\dot{m}_{ev}}{4\pi R_0^2 \rho_f}, \\ Z_2 = \frac{\dot{m}_{ev}}{4\pi R_0^2 \rho_f} \frac{1}{\left(1 + (\varepsilon^2 - 1)\sin^2\theta_1\right)}. \end{cases} \tag{60}$$

Substituting this expression into Eq. (57) gives:

$$\frac{1}{2}\frac{dB}{dt} = \frac{r_1 \dot{r}_1 a_r^2 - r_1^2 a_r \dot{a}_r}{a_r^4} + \frac{z_1 \dot{z}_1 a_z^2 - z_1^2 a_z \dot{a}_z}{a_z^4}$$

$$= \varepsilon^{-1/3} \sin^2\theta_1 \frac{-Z_2 \varepsilon^{4/3} + \varepsilon^{-2/3} Z_1}{R_0 \varepsilon^{-1}} + \varepsilon^2 \cos^2\theta_1 \frac{-Z_2 + Z_1}{R_0 \varepsilon^2}$$

$$= \frac{1}{R_0} \frac{\dot{m}_{ev}}{4\pi R_0^2 \rho_f} \left(\frac{\sin^2\theta_1 (1 - \varepsilon^2) - 1}{\left(1 + (\varepsilon^2 - 1)\sin^2\theta_1\right)} + 1 \right) = 0.$$

Since $B = 1$ at the start of the process, it remains equal to 1 during the development of the process. Hence:

$$B = \frac{r_1^2}{a_r^2} + \frac{z_1^2}{a_z^2} = 1$$

at any time. Thus the shape of the droplet remains spheroidal.

Note that this result refers to isothermal spheroids, which are different to the ones considered in our paper in the general case.

References

[1] S.S. Sazhin, Droplets and Sprays, Springer, Heidelberg, 2014.
[2] E. Michaelides, Particles, Bubbles and Drops, World Scientific, New Jersey, 2006.
[3] C. Crua, M.R. Heikal, M.R. Gold, Microscopic imaging of the initial stage of diesel spray formation, Fuel 157 (2015) 140–150.
[4] S. Tonini, G. Cossali, An exact solution of the mass transport equations for spheroidal evaporating drops, Int. J. Heat Mass Transfer 60 (2013) 236–240.
[5] C. Niven, On the conduction of heat in ellipsoids of revolution, Philosoph. Trans. Roy. Soc. London 171 (1880) 117–151.
[6] M. Jog, M. Hade, Transient heat transfer to a spheroidal liquid drop suspended in an electric field, Int. J. Heat Fluid Flow 18 (1997) 411–418.
[7] D. Lima, S. Farias, G. Lima, Mass transport in spheroids using the Galerkin method, Br. J. Chem. Eng. 21 (2004) 667–680.
[8] R. Alassar, Forced convection past an oblate spheroid at low to moderate Reynolds numbers, ASME J. Heat Transfer 127 (2005) 1062–1070.
[9] A. Richter, P. Nikrityuk, Drag forces and heat transfer coefficients for spherical, cuboidal and ellipsoidal particles in cross flow at sub-critical Reynolds numbers, Int. J. Heat Mass Transfer 55 (2012) 1343–1354.
[10] N. Kishore, S. Gu, Momentum and heat transfer phenomena of spheroid particles at moderate Reynolds and Prandtl numbers, Int. J. Heat Mass Transfer 55 (2011) 2595–2601.
[11] B. Sreenivasulu, B. Srinivas, K.V. Ramesh, Forced convection heat transfer from a spheroid to a power law fluid, Int. J. Heat Mass Transfer 70 (2014) 71–80, http://dx.doi.org/10.1016/j.ijheatmasstransfer.2013.10.065.
[12] B. Sreenivasulu, B. Srinivas, Mixed convection heat transfer from a spheroid to a Newtonian fluid, Int. J. Therm. Sci. 87 (2015) 1–18, http://dx.doi.org/10.1016/j.ijthermalsci.2014.08.002.
[13] G. Juncu, Unsteady heat transfer from an oblate/prolate spheroid, Int. J. Heat Mass Transfer 53 (2010) 3483–3494.
[14] D. Grow, Heat and mass transfer to an elliptical particle, Combust. Flame 80 (1990) 209–213.
[15] J. Li, J. Zhang, A theoretical study of the spheroidal droplet evaporation in forced convection, Phys. Lett. A 378 (47) (2014) 3537–3543, http://dx.doi.org/10.1016/j.physleta.2014.10.020.
[16] V. Zubkov, G. Cossali, S. Tonini, C. Crua, S. Sazhin, Mathematical modelling of heating and evaporation of a spheroidal droplet, in: ILASS, Brighton, 2016.
[17] S. Tonini, G. Cossali, An analytical model of liquid drop evaporation in gaseous environment, Int. J. Therm. Sci. 57 (2012) 45–53.
[18] S.S. Sazhin, M. Al Qubeissi, R. Nasiri, V. Gunko, A. Elwardany, F. Lemoine, F. Grisch, M. Heikal, A multi-dimensional quasi-discrete model for the analysis of Diesel fuel droplet heating and evaporation, Fuel 129 (2014) 238–266.
[19] B. Abramzon, S.S. Sazhin, Convective vaporization of a fuel droplet with thermal radiation absorption, Fuel 85 (1) (2006) 32–46.
[20] S.S. Sazhin, I.N. Shishkova, M. Al Qubeissi, A self-consistent kinetic model for droplet heating and evaporation, Int. J. Heat Mass Transfer 93 (2016) 1206–1217.
[21] F.P. Incropera, D.P. Dewitt, Fundamentals of Heat and Mass Transfer, John Wiley and Sons, 2002.
[22] O. Rybdylova, M. Al Qubeissi, M. Braun, C. Crua, J. Manin, L.M. Pickett, G. de Sercey, E.M. Sazhina, S.S. Sazhin, M. Heikal, A model for droplet heating and its implementation into ANSYS Fluent, Int. Commun. Heat Mass Transfer 76 (2016) 265–270, http://dx.doi.org/10.1016/j.icheatmasstransfer.2016.05.032.
[23] S.S. Sazhin, V. Gunko, R. Nasiri, Quantum-chemical analysis of the processes at the surfaces of diesel fuel droplets, Fuel 165 (2016) 405–412.
[24] J.-F. Xie, S.S. Sazhin, B.-Y. Cao, Molecular dynamics study of the processes in the vicinity of the n-dodecane vapour/liquid interface, Phys. Fluids 23 (11) (2011) 112104.
[25] R. Bird, W. Stewart, E. Lightfoot, Transport Phenomena, second ed., John Wiley and Sons, 2002.
[26] S. Tonini, G. Cossali, One-dimensional analytical approach to modelling evaporation and heating of deformed drops, Int. J. Heat Mass Transfer 97 (2016) 301–307.